J Mater Sci (2015) 50:2832–2848
DOI 10.1007/s10853-015-8845-z

Dy(III) recovery from dilute solutions using magnetic-chitosan nano-based particles grafted with amino acids

Ahmed A. Galhoum · Asem A. Atia · Mohammad G. Mahfouz · Sayed T. Abdel-Rehem · Nabawia A. Gomaa · Thierry Vincent · Eric Guibal

Received: 21 November 2014 / Accepted: 29 December 2014 / Published online: 29 January 2015

Abstract Magnetic-chitosan nano-based particles were successfully prepared by a simple one-pot co-precipitation method before being functionalized with three different amino acid groups (i.e., alanine, serine, and cysteine) using epichlorohydrin as the linking agent. The structural and functional characteristics of the nanosorbents were investigated by elemental analysis, Fourier transform infrared spectrometer, X-ray diffraction, TEM, and vibrating sample magnetometry. The sorption properties of these materials were tested for Dy(III) recovery from aqueous solution: pH effect, uptake kinetics, and sorption isotherms were investigated. Sorbent particles are super-paramagnetic and their size is in the range of 15–40 nm. Kinetic profiles are successfully modeled with the pseudo second-order rate equation. The Langmuir and the Dubinin–Radushkevich equations fit well-sorption isotherms. The maximum sorption capacities at pH 5 (optimum pH, and at T: 27 ± 1 °C) are close to 14.8, 8.9, and 17.6 mg Dy g^{-1} for alanine, serine, and cysteine type, respectively. Cationic species RE(III) in aqueous solution appear to be sorbed by combined chelation and anion-exchange mechanisms. The sorption process begins at low-metal concentration by a physical monolayer sorption at low ion concentration before metal ions can be sorbed at higher metal concentration by coordination. The values of the thermodynamic parameters $\Delta G°$ and $\Delta H°$ indicate the spontaneous and endothermic nature of the mechanism, while the positive values of $\Delta S°$ show that during the sorption process the randomness increases. Finally, the sorbent can be efficiently regenerated using acidified thiourea: the amount of Dy(III) sorbed is hardly reduced, at least during the first four sorption/desorption cycles.

Electronic supplementary material The online version of this article (doi:10.1007/s10853-015-8845-z) contains supplementary material, which is available to authorized users.

A. A. Galhoum · T. Vincent · E. Guibal (✉)
Centre des Matériaux des Mines d'Alès, Ecole des mines Alès, 6 Avenue de Clavières, 30319 Alès Cedex, France
e-mail: Eric.Guibal@mines-ales.fr

A. A. Galhoum (✉) · M. G. Mahfouz · N. A. Gomaa
Nuclear Materials Authority, El-Maadi, P.O. Box 530, Cairo, Egypt
e-mail: Galhoum_nma@yahoo.com

A. A. Atia
Chemistry Department, Faculty of Science, Menoufia University, Shebin El-Kom, Egypt

S. T. Abdel-Rehem
Chemistry Department, Faculty of Science, Ain Shams University, Cairo, Egypt

Introduction

The evolution of international regulations on pollutant discharge from industry into water bodies has focused research on the removal of hazardous species such as heavy metals including, for example, cadmium, lead [1, 2], mercury [3], and chromium(VI) [4]. However, these waste streams can also contain valuable metals such as platinum-group metals [5, 6], silver, gold [7], gallium, indium, rare-earth elements (REEs) [8–12], or uranium [13, 14]. The recovery of valuable metals from dilute aqueous waste streams processing from acid mine drainage, coal mines [15], from industrial effluents, or from treatment of spent materials (wastes and end-of-life consumer goods) comes like complementary to primary mining resources [14, 16, 17].

The removal of metal ions from aqueous streams may use processes such as precipitation, membrane separation, or solvent extraction. However, these processes frequently face technical (solubility limits vs. expected treatment levels), environmental (sludge production, loss of diluent and extractant [18]) or economic (cost vs. concentration levels) constraints that limit their application for the treatment of dilute effluents. For these reasons, in the case of low-metal concentrations, ion exchange or chelating resins are generally preferred [18, 19]. Being an effective separation technique, solid-phase extraction (SPE) has risen to the forefront among the processes that have been extensively carried out in the field of separation and analysis [19, 20]. In addition, SPE provides alternative opportunities not only for the removal of heavy metals from wastewater [1–4] but also for the recovery of precious or strategic metals [8, 21], including uranium [14, 19]. SPE has a number of advantages over other processes: minimal solvent use, flexibility, high concentration factor that made the technique especially attractive for separation and removal of metal ions over the last decade [9, 22]. Biosorption making profit of agriculture or fisheries residues, or from bacterial biomass that bears reactive functional groups similar to those found on synthetic resins can be efficiently used as alternative sorbents [23–25].

A lot of polymer materials have been applied to separate metal ions. Attention has been focused on chitin, chitosan, and their derivatives because they are abundant biopolymers, renewable, and safe (being readily biodegradable). Chitosan is commercially obtained by partial deacetylation of chitin with a strong alkali solution (sodium hydroxide under heating). This is a copolymer made of glucosamine and *N*-acetyl-D-glucosamine units linked together by β(1→4) glycosidic bonds [26]. Chitosan is quite easily modified by chemical grafting (especially on amine and hydroxyl groups), and the biopolymer is frequently used for developing chelating and ion-exchange resin. The other significant interest of this biopolymer as backbone for these resins is associated to its relatively hydrophilic properties (at least compared to usual synthetic polymers such as polystyrene–divinylbenzene, polyethylene, and polyurethane): this is expected to enhance sorption kinetics in aqueous solutions [27]. The main drawback of chitosan is due to its solubility in acidic solutions (with the remarkable exception of sulfuric acid). However, chitosan can be chemically modified to prevent its dissolution in acidic media. It is often cross-linked to confer better microbiological and chemical resistance [13]. On the other hand, cross-linked chitosan (base material) does not have significant affinity for Ln(III); the only possibility to reach appreciable sorption capacity consists on grafting chelating moieties on the biopolymer backbone [28]. The grafting of new functional group on the backbone of chitosan increases the volumetric density and the kind of sorption sites in order to increase sorption capacity and selectivity for target metals [29]. Compared to the traditional micron-sized supports used in separation process, nano-sized sorbents possess quite good performance due to high-specific surface area and the limitation of resistance to intraparticle diffusion. However, the nanosorbents are generally difficult to separate from aqueous solution by filtration or centrifugation. Making these nanoparticles magnetic helps their phase separation using an external magnetic field [26]. These hybrid materials have recently retained a great attention: the magnetic core is covered by a polymeric shell that provides appropriate functional groups (designed for efficient sorption properties) [30].

REEs are essentially used in Hi-Tech materials such as high strength permanent magnets, laser, automotive catalytic converts, fibers optics/superconductors, and electronic devices. Because of the ongoing development of new advanced technologies, there is an ever-increasing demand for REE in the international markets. In addition, the resources and production zones are concentrated in specific and limited world areas; this makes the recovery of these metals a strategic target. This may explain the interest for recovering these metals from non-conventional resources: recycling of spent electronic devices or waste materials [31, 32].

The most thermodynamically stable form of these elements in aqueous solutions is the trivalent state [33]. RE trivalent ions (classified as hard acids according to Pearson's rules due to their high oxidation state, low electronegativity, and small ionic size) tend to readily react with the so-called Pearson hard bases (electron donors, with high electronegativity and low polarizability) such as oxygen, nitrogen, sulfur, and phosphorus atoms [26]. The main challenge in the RE industry is the separation of these metals from heavy metal ions, and their separation from each over (because of their very close chemical properties). Elaborating new sorbing materials with different chemical groups having a different affinity for REEs is thus an important objective for lanthanide-based industry in terms of separation, recovery, and recycling [33]. Chelating or coordinating resins that bear one or more donor atoms may thus represent interesting materials for binding metal ions [34]. In chelating resins, the functional groups the most frequently used are nitrogen (i.e., N present in amines, azo groups, amides, nitriles), oxygen (i.e., O present in carboxylic, hydroxyl, phenolic, ether, carbonyl, phosphoryl groups), and sulfur (i.e., S present in thiols, thiocarbamates, thio-ethers). Usually, the anchored molecules contain nitrogen, oxygen, or sulfur atoms, or a combination of them; they are acting as basic complexing groups. Their "spatial arrangement," in the best cases, allows these resins to have interesting selective extraction properties [35].

Several chelating ligands such as catechol, iminodiacetic acid, iminodimetyl-phosphonic acid, phenylarsonic acid, or serine [9], and amino acids moieties (glycine, valine, leucine, and serine) [22] were used to functionalize cross-linked chitosan for sorption of lanthanide metal ions. Thus, to further facilitate the sorption affinity, surface modification, including physical coating and covalent binding, has often been explored to enable specific metal complexation.

This study focuses on the recovery of Dy(III), selected as a representative of trivalent lanthanide family, using three derivatives of chitosan (obtained by grafting of amino acids). Covalent attachment of chelating groups such as amino acids moieties to the surface of magnetic nanoparticles was achieved to study the structure/activity relationships between alanine (a "simple" amino acid), serine (a hydroxyl-bearing amino acid) and cysteine (a thiol-bearing amino acid). Magnetic-chitosan support was manufactured using (a) Fe_3O_4 nanoparticles as magnetic core, and (b) chitosan as the coating support (which was functionalized with amino acids). Amino acid grafting was performed using epichlorohydrin as the linking agent between amino acid and chitosan.

The structural and functional characteristics of the nano-sized magnetic sorbents were investigated by elemental analysis, FTIR, XRD, and TEM. The magnetic properties were measured using a vibrating sample magnetometer (VSM). Dysprosium(III) sorption was investigated in batch with a special attention paid to pH and temperature effects, uptake kinetics, and sorption isotherms. Metal desorption and sorbent recycling were also investigated.

Materials and methods

Reagents and analysis

Chitosan (90.5 % deacetylation) was supplied by Sigma-Aldrich (France). Alanine, serine, and cysteine were obtained from Sigma-Aldrich; epichlorohydrin (>98 %), 1,4-dioxane (99.9 %), and ethanol were purchased from Fluka. Sodium hydroxide solution (30 % w/w) was supplied by Chem-Lab. NV and all other chemicals were Prolabo products and were used as received.

Rare-earth solution

$DyCl_3.xH_2O$ was purchased from Sigma-Aldrich and was burned off at 900 °C for 3 h. Stock solution of Dy(III) was prepared by dissolving the burnt salt in concentrated sulfuric acid under heating before being diluted with demineralized water until final concentration of 1000 mg Dy L^{-1}. The working solutions were prepared by appropriate dilution of the stock solutions immediately prior to use. The metal concentrations in both initial and withdrawn samples were determined by an Inductively Coupled Plasma Atomic Emission Spectrometer (ICP-AES JY Activa M, Jobin–Yvon, Longjumeau, France).

Preparation of sorbent

Preparation of cross-linked chitosan–magnetite nanocomposites

Chitosan–magnetite nanocomposites were prepared by chemical co-precipitation of Fe(II) and Fe(III) ions by NaOH in the presence of chitosan followed by treatment under hydrothermal conditions (the so-called Massart method) [36, 37]. Chitosan (4 g) was dissolved in 200 mL (20 %) acetic acid before dissolving $FeSO_4$ and $FeCl_3$ salts (added under 1:2 molar ratio). The ratio of magnetite to chitosan was 1:1 (i.e., for 4 g of chitosan, 6.62 g of $FeSO_4.7H_2O$, and 8.68 g of $FeCl_3$). The resulting solution was chemically precipitated at 40 °C by adding 2 M NaOH dropwise with constant stirring, at controlled pH (10–10.4). The suspension was heated at 90 °C for 1 h under continuous stirring and separated by decantation. Then, a solution of 0.01 M epichlorohydrin containing 0.067 M sodium hydroxide was prepared (pH 10) and added to freshly prepared wet magnetite-chitosan in a ratio of 1:1 (i.e., for 4 g (or 0.024 mmol N) of chitosan in the mixture chitosan-magnetite 0.024 mmol epichlorohydrin). The mixture of chitosan–magnetite and epichlorohydrin was heated to a temperature between 40 and 50 °C for 2 h under continuous stirring [38]. After 2 h of reaction time, the products were filtered and extensively washed with distilled water to remove unreacted epichlorohydrin.

The amino acid moiety (alanine/serine/cysteine) was introduced to the cross-linked magnetic-chitosan in two steps [39]. First, the epichlorohydrin-cross-linked magnetic-chitosan product was suspended in 150 mL ethanol/water mixture (1:1 v/v). Epichlorohydrin (15 mL) was then added to the suspension, and the mixture was refluxed for 4 h. After the reaction, the product was filtered and washed each three times with ethanol and with ultrapure water to remove any residual reagent. In a second step, the epichlorohydrin-activated material was suspended in dioxane (200 mL) in the presence of amino acid (16 g of either alanine, serine, or cysteine, for an initial amount of 4 g of chitosan). The pH of the suspension was adjusted to 9.5–10 with 1 M NaOH solution and refluxed for 6 h. After the reaction, the final product was filtered and washed three times with ethanol and with ultrapure water. Finally, the final product was freeze-dried for about 24 h.

The amine content in the sorbent was estimated using a volumetric method as follows [21]: 30 mL of 0.05 M HCl solution was added to 0.1 g of material and conditioned for

15 h on a reciprocal shaker. The residual concentration of HCl was estimated through titration against 0.05 M NaOH solution and phenolphthalein as indicator. The number of moles of HCl having interacted with amino group, and consequently the concentration of amino group (mmol g^{-1}) were calculated using Eq. (1)

$$\text{Concentration of amino group} = (M_1 - M_2) \times 30/0.1 \quad (1)$$

where M_1 and M_2 are the initial and final concentrations of HCl, respectively.

Characterization methods

The chemical composition (carbon, hydrogen, and nitrogen contents) of the resins was characterized using an automatic analyzer (CHNS Vario EL III-elementar analyzer, Elementar, Germany). Powder X-ray diffraction (XRD) patterns were obtained at room temperature by a Philips X-ray generator model with a PW 3710/31 control X-ray diffraction system (Philips, The Netherlands), using Cu K_α radiation in the range of $2\theta = 10$–$90°$. The dimensions and morphologies of the sorbents were observed by high-resolution transmission electron microscope-HRTEM (JEOL-2100, Japan). Their magnetic properties were measured on a VSM (730T, Lakeshoper, America) at room temperature. Functional groups of sorbent were analyzed with a Fourier transform infrared spectrometer (FTIR spectrometer: Nicolet Nexus 870 FTIR, Nicolet, USA). The analytical scanning range was set between 4000 and 400 cm^{-1}, and the analyses were performed on the samples conditioned under the form of KBr pellets.

Sorption experiments

Batch experiments were carried out by contact of 20 mg of functionalized chitosan sorbent with 100 mL of aqueous metal ion solution (100 mg Dy L^{-1}) at fixed initial pH in polypropylene centrifuge tube, under agitation (300 rpm) and at 300 K for 4 h. After equilibration and phase separation, the pH was recorded, and the residual metal concentration in the aqueous phase was estimated by ICP–AES, while the concentration of metal ions sorbed onto the functionalized chitosan was obtained by the mass balance equation, Eq. (2)

$$q = \left(C_0 - C_{eq}\right) \times V/M \quad (2)$$

Here q is the amount of sorbed metal ions (mg Dy g^{-1} sorbent), while C_0 and C_{eq} are the initial and equilibrium metal ion concentrations (mg Dy L^{-1}) in the aqueous solution, respectively. V is the volume of the solution (0.02 L) and M is the mass of the sorbent (0.05 g).

For the study of sorption properties, several parameters were successively investigated: (1) the influence of pH, (2) uptake kinetics, (3) sorption isotherm, (4) the influence of temperature, and (5) metal desorption and sorbent recycling.

Isotherm studies were investigated by mixing 0.05 g of sorbent with 20 mL of Dy(III) solution at different initial concentrations (i.e., 25, 50, 75, 100, 150, 200, and 300 mg L^{-1}, at pH 5) and shaking for 4 h at 300 rpm. The experiments were performed in a thermostatic chamber, at different temperatures (300 ± 1, 310 ± 1 and 320 ± 1 K, respectively). Uptake kinetics was performed using a sorbent dosage of 2.5 g L^{-1} and a concentration of 100 mg Dy L^{-1} at 300 ± 1 K: samples were collected under agitation at standard times and metal concentration was determined, after magnetic separation, by ICP–AES.

Thiourea (0.5 M) acidified with few drops of H_2SO_4 (0.2 M) was chosen as the eluent for the study of metal desorption. The contact time between the eluent and the metal-loaded sorbent was set to 1 h (under constant agitation). The sorption yield after regeneration for three cycles was compared to the value reached for the first cycle.

The duplication or triplication of selected experiments showed that the standard deviation was systematically less than 5 %.

Results and discussion

Preparation of magnetic-chitosan nanoparticles

A simple one-step in situ co-precipitation method was used to synthesize magnetic-chitosan nanoparticles. Under selected experimental conditions, magnetite particles were spontaneously produced, the pH change caused the simultaneous chitosan co-precipitation and embedding of magnetic nanoparticles. In addition, the dropwise addition of NaOH in the chitosan/Fe(II)/Fe(III) mixture under constant stirring leads to the formation (and stabilization) of nanometric-sized chitosan-magnetite composite particles [37]. To prevent the loss of amine groups (and sorption capacity), epichlorohydrin (chloromethyloxirane) was preferred to aldehyde for chitosan cross-linking. Indeed, the cross-linking with glutaraldehyde involves reaction on amine functions that loss, at least partially, their complexation properties [40]. The epichlorohydrin-activated material was then reacted with amino acid (alanine, serine, or cysteine). Although the cross-linking agent could react with different functional groups (such as amine groups and hydroxyl groups), FTIR analysis (see below) showed that the hydroxyl groups appear to be the groups preferentially influenced by the grafting of spacer groups (in the intermediary stage of the synthesis procedure, the bands representative of hydroxyl groups were attenuated). This is consistent with the description of the synthesis route proposed by Dong et al. [41] for the

formation of epichlorohydrin-cross-linked chitosan magnetic particles: the presence of iron salts (Fe(II) and Fe(III) ions) in the chitosan solution suggests the possible interaction of these ions with amino groups, which, in turn, are "protected." Under these conditions, the cross-linking agent will preferentially react with hydroxyl groups. The protection of amino groups by weak interaction with iron leads to cross-linking with epichlorohydrin at the level of $–CH_2OH$ groups as already reported by Dong et al. [41]. On the other hand, when the spacer arm (epichlorohydrin) is grafted on cross-linked hybrid chitosan magnetic particles in water/ethanol solution, the cross-linking agent reacts with remaining amino groups, leaving –Cl ends that can react further with amino acids. In alkaline dioxane solutions (under heating), the reaction may take place preferentially (with chlorine release) (a) with amino groups in the case of alanine since other reactive groups (i.e., $–CH_3$) are poorly reactive; (b) with amino groups and $–CH_2OH$ groups in the case of serine, and (c) with amino groups and $–CH_2SH$ groups in the case of cysteine. The synthesis reaction suspected to occur for the chemical modification is a typical SN2 reaction that takes place between nucleophilic sites on the amino acid (i.e., $–NH_2$ and –OH or –SH) and the carbon associated to Cl element. This reaction is favored by the alkaline aprotic solvent. Carboxylic groups are electron-withdrawing sites that contribute to displace the ion pair of electrons on nitrogen from amino groups making these groups less nucleophilic: this may explain that the grafting occurs, when possible, with alternate groups such as –OH or –SH (for serine and cysteine, respectively) preferentially to $–NH_2$ (except in the case of alanine, where $–CH_3$ group is not reactive).

When the amino groups of the amino acid are protected (by benzaldehyde, for example), the grafting is orientated toward reaction with the alternate substituent (i.e., $–CH_2OH$ for serine [42]). In the present case, amino groups have not been protected and the grafting could potentially involve amino groups. However, the FTIR spectra showed a significant increase in the intensity of –NH stretching vibration, while, for example, the stretching vibration of free C–S functional group (expected to appear in the range 630–710 cm^{-1} [43]) is not identified. Although the possibility that some amino groups of the amino acid could be involved in the immobilization, it appears that most of the grafting proceeds through the alternate substituent.

Figure 1 shows the synthesis route for alanine (similar reactions occur with serine and cysteine), while Fig. 2 shows the chemical structure of the different derivatives obtained with alanine, serine, and cysteine.

Characterization of the sorbents

The elemental analysis of the different samples is reported in Table 1. The increase of carbon, hydrogen, nitrogen, and sulfur contents shows the successful grafting of alanine, serine, and cysteine moieties onto cross-linked chitosan-magnetite. To confirm the grafting of amino acid moieties on the chitosan backbone (surface coating), the materials were analyzed by FTIR spectrometry (Fig. 3). The band at 568 cm^{-1} is assigned to Fe–O stretching vibration of Fe_3O_4 [30, 37, 44]. A characteristic strong and broad band appeared at around 3399 cm^{-1} that corresponds to the contributions of stretching vibration of –OH group, stretching vibration of N–H group, and inter hydrogen bonds of polysaccharides in the chitosan-magnetite composite [4]. The characteristic peak of primary amine $–NH_2$ appears at 3399 and 1613 cm^{-1}. The bands at 1463 and 1364 cm^{-1} can be attributed to the C–O–C stretching and –OH bending vibrations, respectively. The absorption band at 893 cm^{-1} is characteristic of β-D-glucose unit [19, 30]. The absorption bands around 1320 and 1065 cm^{-1} correspond to the stretching vibrations of primary –OH group and secondary –OH group, respectively. However, the absorption intensity of $–NH_2$ group and –OH from the cross-linked material is obviously lower than that of the chitosan-magnetite composite: this confirms that the cross-linking reaction occurs between chitosan and epichlorohydrin [19]. The new band at 792 cm^{-1} (comparing to magnetic-chitosan reference material) may be attributed to the $–CH_2–Cl$ stretching vibration [43]. The disappearance of this band while grafting the amino acid confirms that the amino acid binds to the end of the spacer arm. The grafting of amino acids on chitosan is confirmed by the appearance of new bands at 1637, 1638, and 1631 cm^{-1}: they are characteristic of carboxylate groups ($–COO^-$) brought by amino acid moieties [39, 45]. The intensity of bands at 1422, 1411, and 1387 cm^{-1} increases on the spectra of alanine, serine, and cysteine derivatives, respectively: this is associated to the increase in the density of amine groups due to amino acid grafting [4]. The contents of amino groups for alanine, serine, and cysteine-type sorbents were volumetrically determined and found to be 3.94, 3.60, and 3.54 mmol g^{-1}, respectively. This means about 1.38, 1.26, and 1.24 times the amount of amine groups of the cross-linked chitosan-magnetite matrix, respectively.

XRD patterns of alanine-, serine-, and cysteine-functionalized chitosan–magnetite nanoparticles are shown in Fig. 4. Fe_3O_4 was identified by the presence of eight characteristic peaks corresponding to indices: (111), (220), (311), (400), (422), (511), (440), and (622). These peaks are consistent with the database in JCPDS file (PDF No.

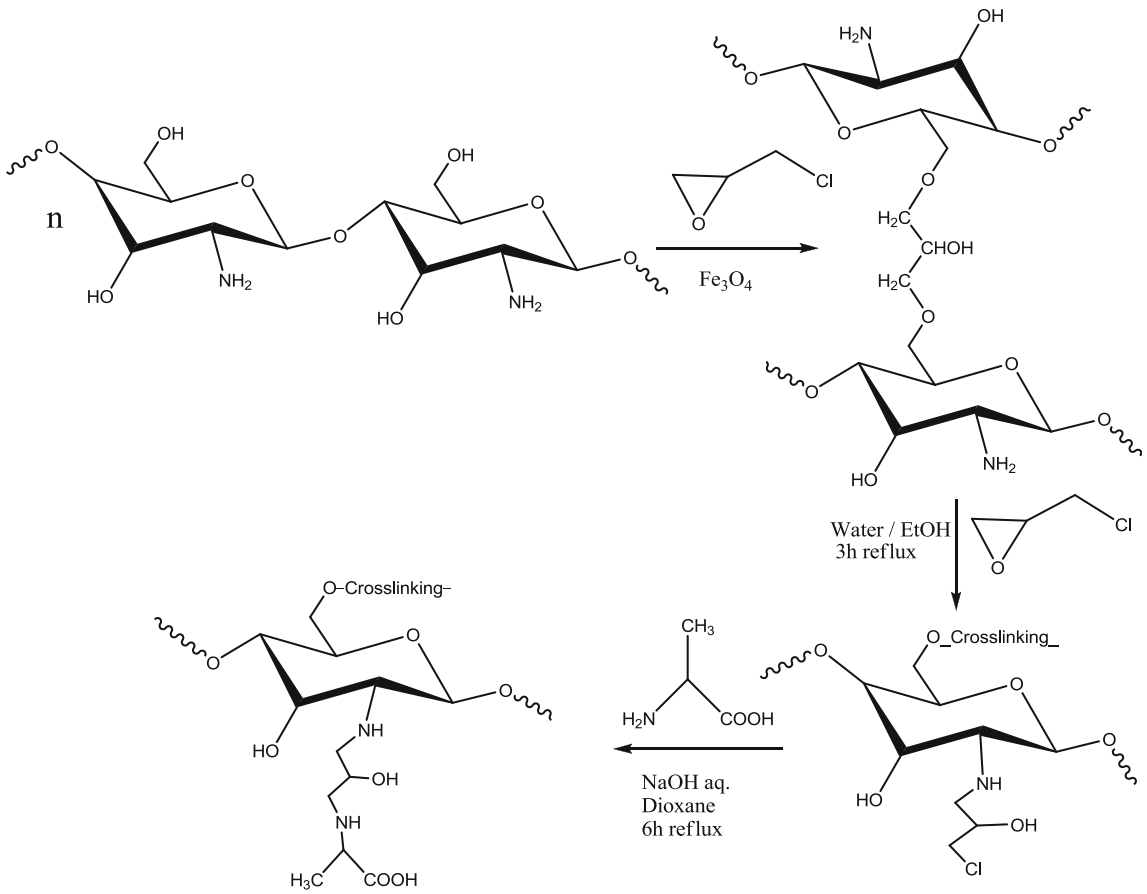

Fig. 1 Scheme for the synthesis of alanine-functionalized magnetic-chitosan nano-based particles

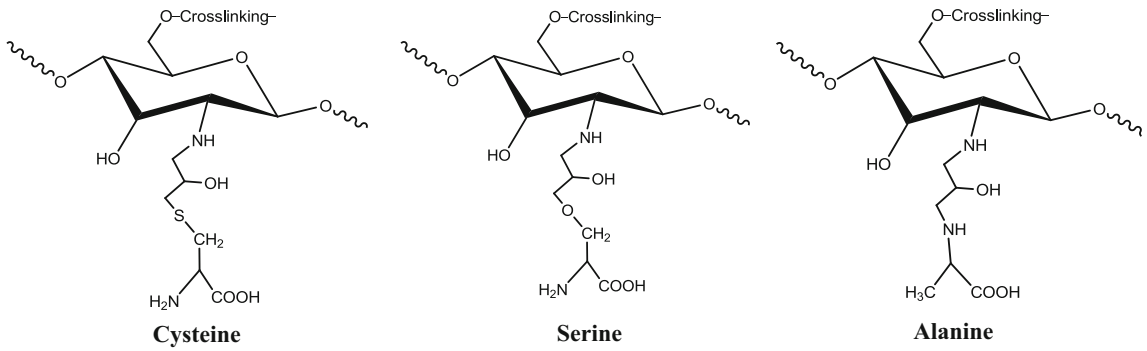

Fig. 2 Structures of alanine-based, serine-based, and cysteine-based sorbents

Table 1 Elemental analysis of the matrix and three sorbents

Sample	C (%)	H (%)	N (%)	S (%)
Matrix	14.23	2.55	1.71	–
Alanine type	17.18	2.66	3.48	–
Serine type	16.19	2.58	3.28	–
Cysteine type	19.84	3.93	3.14	2.34

65-3107) [44], indicating the existence of iron oxide particles (Fe_3O_4) with a spinel structure, which has magnetic properties and can be used for magnetic separation. The Debye–Scherrer equation was used for calculating the size of the nanoparticles (based on the broadening of X-ray diffraction peaks). The half width at half maximum is related to the size of crystals through the equation [46]:

$$D = k\,\lambda/\beta\,\cos\,\theta \qquad (3)$$

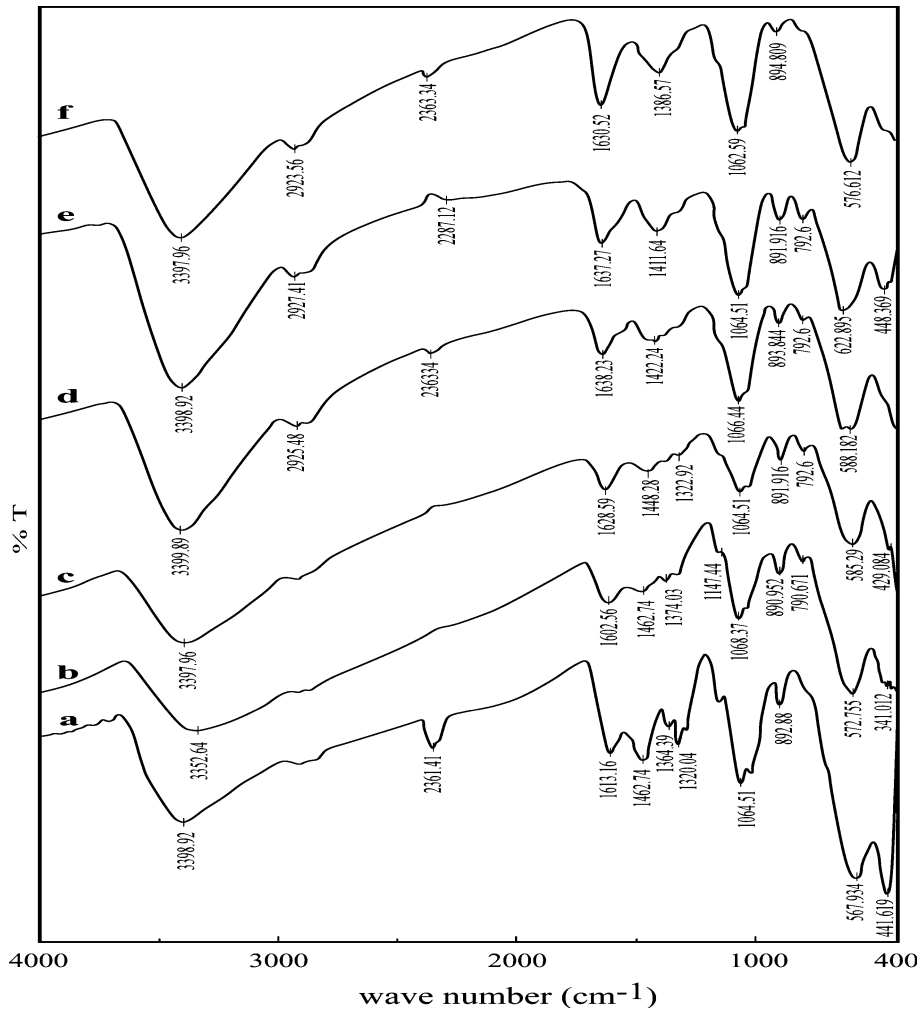

Fig. 3 FTIR spectra of *a* chitosan-magnetite nano-based particles, *b* after cross-linking, *c* cross-linked chitosan–magnetite with spacer arm, *d* serine type, *e* alanine type, and *f* cysteine type

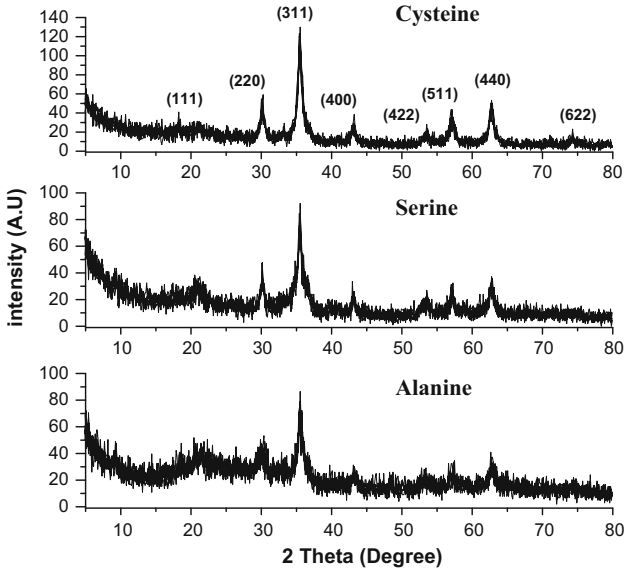

Fig. 4 Powder X-ray diffraction (XRD) patterns of amino acid-functionalized magnetic-chitosan nano-based particles

where D is the average nanoparticles diameter, λ is the wavelength of X-ray radiation (1.5418 Å), θ is the angle of diffraction, $k = 0.9$, and β is the full width at half maximum of X-ray diffraction peaks. Here calculations were performed on the major peak (i.e., corresponding to index (311)). The crystal size has been found to be 13.0, 11.6, and 13.5 nm for alanine-, serine-, and cysteine-functionalized materials, respectively.

The three sorbents have a roughly spherical morphology and are homogeneously distributed (Fig. 5). The structure of the sorbents was globally monodisperse; the average diameter of particles was 15–40 nm. This means about 1–3 times the size of crystals (according XRD analysis): crystals tend to agglomerate (probably under the effect of dipole/dipole magnetic attraction), though the particles remain very small. Moreover, TEM images also showed different contrasts on the materials: the dark areas correspond to crystalline Fe_3O_4, while the bright ones are associated with chitosan.

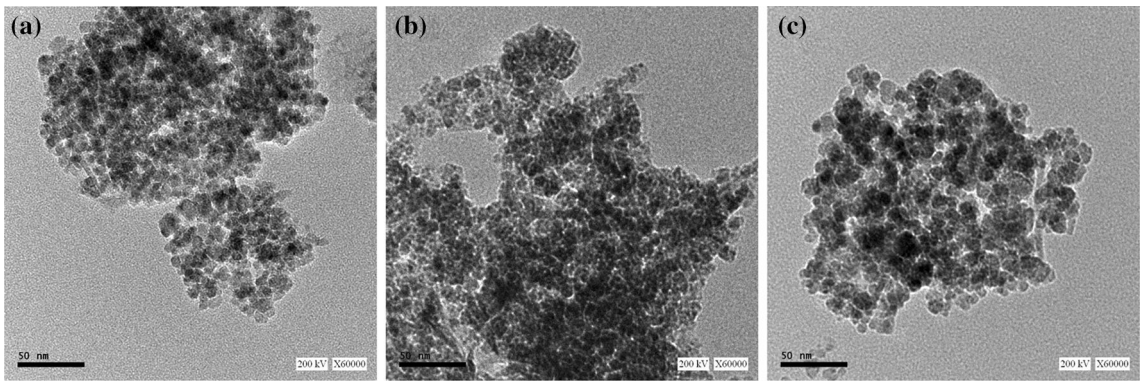

Fig. 5 TEM micrographs (the *bar* corresponds to 50 nm): **a** alanine, **b** serine, and **c** cysteine-functionalized magnetic-chitosan nano-based particles

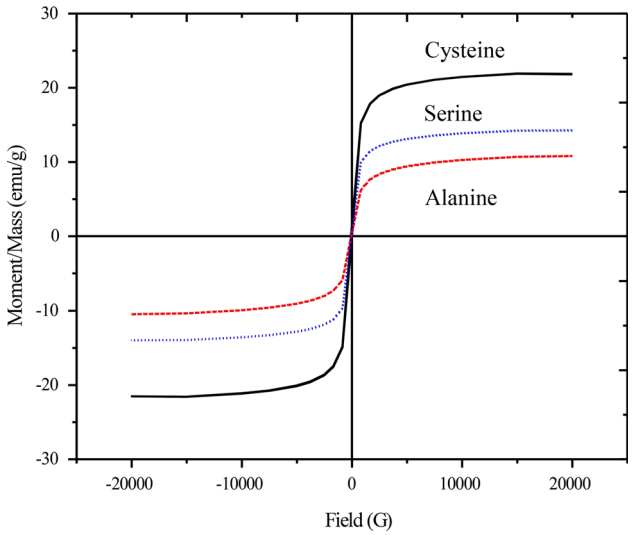

Fig. 6 Magnetization curves of *a* alanine, *b* serine, and *c* cysteine-functionalized magnetic-chitosan nano-based particles

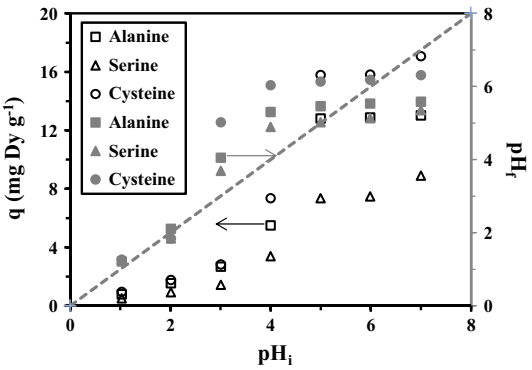

Fig. 7 Effect of pH on the sorption of Dy(III) ions using alanine-, serine-, and cysteine-functionalized magnetic-chitosan nano-based particles: sorption capacity versus initial pH (*open symbols*) and equilibrium pH versus initial pH (*closed symbols*) ($C_0 = 100$ mg Dy L^{-1}; $T = 300$ K; $t = 4$ h; $m = 0.05$ g; $V = 20$ mL)

The magnetic properties of the materials were determined using VSM. Figure 6 shows their typical magnetization loop. There were no remanence and coercivity. The saturation magnetization of alanine-, serine-, and cysteine-functionalized sorbents were found to be about 14.0, 10.6, and 21.5 emu g^{-1}, respectively. These values are significantly lower than the saturation magnetization of bulk magnetite, and this was attributed to the embedment of the magnetic cores into a non-magnetic matrix [47]. Therefore, the magnetic-chitosan nanoparticles can be readily separated with the help of an external magnetic field. The differences are relatively marked for the different materials. They may be due to a difference in the thickness (and amount) of modified polymer coating. Indeed, the grafting of the amino acid is not expected to affect by itself the magnetic behavior of the composite material.

Sorption properties

pH effect

The influence of pH on Dy(III) sorption on the different sorbents has been investigated in the pH range of 1–7 (Fig. 7); above pH 7, dysprosium begins to precipitate as $Dy(OH)_3$. Below pH 1, the sorbent begins to dissolve: both biopolymer and magnetic core may lose stability. Since the pH may change during the sorption process, the final pH was systematically monitored and reported in Fig. 7. Sorption capacities increase with initial pH: below pH 3, the sorption slightly increases; between pH 3 and 5, the sorption sharply increases; while above pH 5 the sorption tends to stabilize. Actually, the weak variation of sorption capacity above pH 5 is due to the "buffering-like" effect of the sorbent: the pH stabilizes around 5.1, 5.5, and 6.2 for serine-, alanine-, and cysteine-functionalized magnetic-chitosan sorbents, respectively. Then the variation of

sorption capacity remains negligible. For further experiments, the pH of solutions was set to pH 5 to minimize pH variation and possible dysprosium precipitation (at high metal concentration) and to reach maximum sorption capacities.

In strong acidic solutions, both carboxyl groups and amino groups of the different sorbents are protonated (see additional material section for pK values of reactive groups), which results in positively charged surface of the sorbents. The competition of protons for binding on reactive sites and the repulsive effect of positively charged surface for Dy(III) binding explain the dramatic decrease of sorption capacities. It is noteworthy that the drastic effect of acidic conditions brings information on the experimental conditions that could be suitable for Dy(III) desorption form-loaded sorbent particles. Using acidic conditions will enhance metal desorption providing material stability is maintained. As the pH increases, the protonated amine and carboxylate groups gradually deprotonate. Therefore, the surface charge on the sorbents (carboxylate functions) turns negative, which significantly enhances the electrostatic interaction between the sorbent and metal cations [14, 48]. The deprotonation of amine groups also makes the free electron doublet of nitrogen available for complexation and coordination with metal ions. Although the general trends were roughly the same for the different sorbents regarding pH dependence, there is a slight shift in the curves with a pH-edge moving to the highest pH according the sequence: serine < alanine < cysteine (Figure AM1, See additional material section). This ranking can be correlated to the pK values of their amino groups (9.15/9.69/10.13 for serine, alanine, and cysteine, respectively).

There are substantial differences in the sorption capacities of the different materials: cysteine (15.8 mg Dy g^{-1}) > alanine (12.8 mg Dy g^{-1}) > serine (7.4 mg Dy g^{-1}). The main differences between the different amino acids consist of their end-groups: $–CH_3$ for alanine, $–CH_2OH$ for serine, and $–CH_2SH$ for cysteine. The improvement of sorption capacity for cysteine-functionalized sorbent was expectable, since the sulfur group is a supplementary reactive group compared to structure of the other amino acids; and sulfur groups are generally very reactive with metal ions. However, the Pearson's rule [49] (see below) indicates that the sulfur has probably a lower affinity for Dy(III) than other reactive groups such as O and N. In addition, the thiol moiety being involved in the grafting of the amino acid to chitosan backbone may affect its reactivity. More surprising is the significant decrease in the sorption capacity of serine- vs. alanine-functionalized materials. Indeed, both $–CH_3$ and $–CH_2OH$ end-groups are poorly reactive for metal binding. For cysteine-functionalized sorbent, metal can be bound by amine groups (free electron doublet on nitrogen), carboxylate groups (chelation or ion exchange), and sulfur or thiol groups (though involved in the grafting of the amino acid on chitosan backbone). For alanine derivative, the reactive groups may be the carboxylate groups and the secondary amine groups (though involved in the grafting of the amino acid on chitosan backbone): in this case, the secondary amine groups are probably less reactive for binding Dy(III) than in the case of cysteine-based sorbent, due to steric hindrance and less favorable electron donor/acceptor properties. In the case of serine-functionalized sorbent, the steric hindrance may explain the weaker efficiency of the sorbent for binding Dy(III) ions compared to alanine-based sorbent. Dy(III) ions are supposed to form chelates with the secondary amino group (–NH–) and the carboxyl group (–COOH) in alanine type chitosan resin due to the absence of steric hindrance, while Dy(III) ions might be more difficult to form a chelate with the primary amino group ($–NH_2$) and the carboxyl group (–COOH) in the serine-type chitosan resin [39]. In addition, the differences in sorption capacity of Dy(III) ions for the different amino acids could be related to the electronegativity of these reactive groups. The sorption profile of these metal ions can be interpreted according to the theory of hard and soft acids and bases (HSAB) defined by Pearson [49]: hard acids (low polarizability and high electronegativity) prefer to associate with hard bases (N, O, F), while soft acids (high polarizability and low electronegativity) prefer to associate with soft bases (P, S, I). For example, Pearson described the interactions of *d* orbital on the metal atom with the *p* orbital of the hydrogen donor in function of the hard/soft nature of the binding: for hard acid/hard base interaction, the *d* orbital is empty and the *p* orbital is filled (while for soft/soft interaction the *d* orbital is filled and the *p* orbital is empty). Actually, lanthanides form hard Lewis acid cations and they have strong affinity to hard Lewis base ligand molecules (containing O and N donors) [50]. Yang and Alexandratos [51] reviewed the literature on polymer-supported reagents for the recovery and separation of lanthanides. They correlate the affinity of the sorbents with donor atom polarizability. They comment that if the HSAB is an important determinant of ion-ligand (reactive group) affinity, other factors may contribute to change the binding performance: geometrical constraints (the longer the spacer arm, the better the reactivity) and the binding mechanism (complexation/chelation vs. ion exchange). In this case, the additional factors that can affect the affinity order between the lanthanides are as follows: (a) the basicity or polarizability of the ligand versus the acidity or polarizability of the ion, (b) the protonation of the ligand, (c) the association of the metal ions with counter ions, and (d) the extent of hydration of ions (hydration enthalpy). All these reasons may explain that the trends observed in the present study

are not as clear as expected from the simple application of the HSAB theory.

Effect of contact time and kinetic studies

Uptake kinetics is another fundamental aspect for the evaluation of the sorption properties of the sorbent. Sorption reactions usually involve multistep mechanisms comprising [52]: (1) bulk diffusion, (2) external film diffusion, (iii) intraparticle diffusion, and (4) proper sorption reaction between sorbate and active sites. From the plots of $q(t)$ versus t as shown in Fig. 8, it can be seen that the sorption rates were fast and over 52 % of total sorption occurred within the first 15 min. In addition, the sorption equilibria of the three sorbents were achieved within 4–6 h, under selected experimental conditions.

The uptake kinetics has been analyzed by various kinetic models, such as the pseudo first-order rate equation (PFORE) (Eq. 4), the pseudo second-order rate equation (PSORE) (Eq. 5), and the resistance to intraparticle diffusion (RIDE) equation [52].

$$q(t) = q_e\left(1 - e^{-k_1 t}\right) \tag{4}$$

$$q(t) = \frac{k_2 \times q_e^2 \times t}{1 + k_2 \times q_e \times t} \tag{5}$$

where q_e and $q(t)$ (mg Dy g^{-1}) are the sorption capacities at equilibrium and time t (min), respectively; k_1 (min^{-1}) and k_2 (g mg^{-1} min^{-1}) are the rate constant of PFORE and PSORE, respectively. The constants of the models (Table 2) have been determined using the non-linear fitting package of Mathematica® software.

The resistance to intraparticle diffusion can be described, in a simplified approach, by Eq. (6)

$$q_t = k_{int.} t^{0.5} + c \tag{6}$$

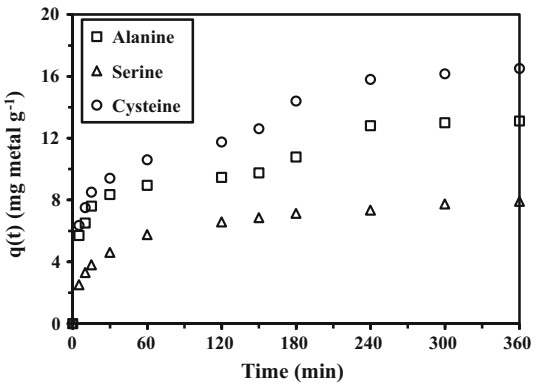

Fig. 8 Dy(III) uptake kinetics for alanine-, serine-, and cysteine-functionalized magnetic-chitosan nano-based particles (C_0 = 100 mg Dy L^{-1}; T = 300 K; pH = 5; sorbent dosage: 2.5 g L^{-1})

where $k_{int.}$ (mg g^{-1} $min^{-0.5}$) is the intraparticle diffusion constant.

The experimental data have been systematically modeled by the aforementioned kinetic equations; the parameters of these models are listed in Tables 2 and 3. Based on the analysis of the estimated variance (Table 2), the PSORE gave a better fit of experimental data for the three sorbents compared to PFORE. This conclusion is confirmed by the comparison of equilibrium sorption capacities (q_e): the q_e calculated by the PSORE was systematically closer from the experimental q_e than the values obtained with the PFORE, regardless of the sorbent. Actually, the sorption can be described as a two phase process: (a) about 50 % of the sorption occurred within the first 15 min of contact (corresponding to a physical sorption mechanism), followed by (b) chemical sorption involving charge neutralization, coordination, and chelation [4] till equilibrium. Chitosan, used as powder or particles, is generally considered as a poorly porous material: this induces significant resistance to intraparticle diffusion. However, in the present case, chitosan is deposited as a thin coating layer at the surface of magnetite particles (of nanometric size): the limitations for intraparticle diffusion are thus limited [14]. For this reason, RIDE is not expected to be the rate-controlling step of the sorption process. This is consistent with the test of modeling of experimental data with the RIDE model (Table 3 and Figure AM2, See Additional Material Section). On the plot of $q(t)$ versus $t^{0.5}$, two sections are identified: (a) within the first 30 min of contact a linear section (corresponding to the possible effect of resistance to film diffusion), (b) followed by a quasi-linear section associated to resistance to intraparticle diffusion regime (which counts for marginal sorption).

The PSORE and the PFORE models have been initially designed for describing chemical reaction kinetics. These models are frequently tested for fitting experimental data in heterogeneous systems and more specifically for describing sorption processes. However, in these cases, the rate parameters (k constant) should be considered as "apparent" parameters, since they integrate the unknown contribution of the mechanisms of resistance to diffusion (both external and intraparticle diffusion). Plazinski et al. [53] reported that under certain (simple) conditions, the PSORE model can be described in terms of intraparticle diffusion model. However, in the present study, the thickness of the modified chitosan layer on the magnetic nano-based particles considerably reduces the potential impact of resistance to intraparticle diffusion. Thus, the parameters determined in fitting experimental data approach intrinsic reaction rates.

This section leads to the conclusion that uptake kinetics can be described by the PSORE. The chemisorption is the rate-controlling step that involves valence forces through

Table 2 Kinetics parameters of pseudo first-order and pseudo second-order models for Dy(III) sorption at 27 °C and pH 5

Adsorbent	$q_{max.\ exp.}$ (mg Dy g^{-1})	PFORE			PSORE		
		$k_1 \times 10^2$ (min^{-1})	q_e (mg Dy g^{-1})	EV	$k_2 \times 10^3$ (g mg^{-1} min^{-1})	q_e (mg Dy g^{-1})	EV
Alanine	13.1	8.80	10.9	2.65	10.1	11.8	1.59
Serine	7.9	4.74	7.10	0.43	8.15	7.77	0.13
Cysteine	16.5	6.24	13.9	4.43	5.29	15.2	2.40

EV estimated variance (Mathematica®)

Table 3 Kinetics parameters of intraparticle diffusion models for Dy(III) sorption at 27 °C and pH 5

Adsorbent	RIDE		
	c (mg g^{-1})	$k_{int.}$ (mg g^{-1} $min^{-0.5}$)	R^2
Alanine	3.89	0.535	0.845
Serine	1.91	0.366	0.889
Cysteine	4.13	0.721	0.898

sharing or exchange of electrons between the sorbent surface and adsorbate ions. The resistances to film diffusion and intraparticle diffusion have a negligible effect on uptake kinetics [13].

Sorption isotherms

Sorption isotherms describe the equilibrium distribution of Dy(III) between the liquid and the solid phases for different metal concentrations (Fig. 9); this curve may help in understanding the controlling mechanisms and quantifying the sorption properties of the sorbent: maximum sorption capacity and affinity of the sorbent for the target metal [54]. All the curves, regardless of the sorbent and the temperature, show similar trend: a progressive increase of sorption capacity (up to a residual metal concentration in the range 100–120 mg Dy L^{-1}), followed by the saturation of the sorbent. The saturation plateau gives a first trend on the mechanisms that could be involved in metal binding. The sorption of Dy(III) ions occur as a monolayer. The sorption equilibrium data have been analyzed by various isotherm models, such as Langmuir, Freundlich, Temkin, and Dubinin–Radushkevich (D–R) equations [55].

Langmuir model is based on the assumption that sorption sites are identical and energetically equivalent, and that the solute is immobilized under the form of monolayer coverage [54]. It can be represented, after linearization, by Eq. (7)

$$\frac{C_{eq}}{q_e} = \frac{C_{eq}}{q_{max}} + \frac{1}{b\,q_{max}} \tag{7}$$

where C_{eq} is the equilibrium metal ion concentration in the aqueous (mg Dy L^{-1}), q_{max} is the maximum sorption

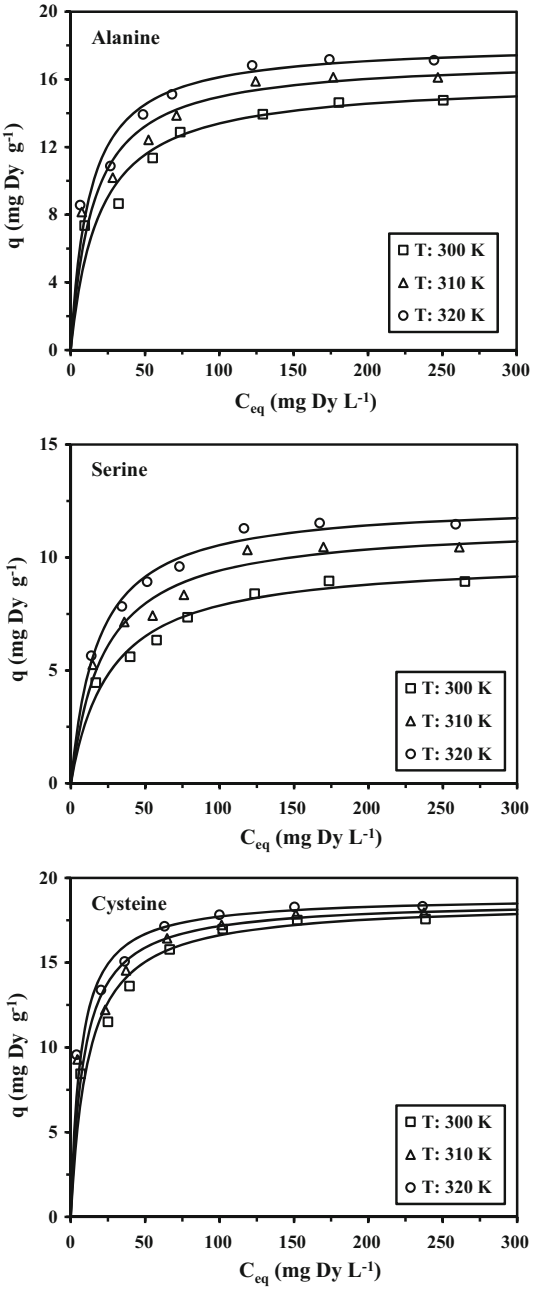

Fig. 9 Sorption isotherms of Dy(III) ions at different temperatures using alanine-, serine-, and cysteine-functionalized magnetic-chitosan nano-based particles ($t = 4$ h; pH = 5; $m = 0.5$ g; $V = 20$ mL; *solid lines* simulation of isotherm with the Langmuir equation and parameters from Table 4)

capacity of the sorbent (mg g^{-1}), and b is the Langmuir sorption constant (L mg^{-1}).

Freundlich isotherm model is based on the assumption of an exponential diminution of sorption site energy [55, 56]. It is applied to describe heterogeneous system characterized by a heterogeneity factor of n. The Freundlich model is described, after linearization, by Eq. (8)

$$\ln q_e = \ln K_f - \frac{1}{n} \ln Ceq \tag{8}$$

where K_F and n are the Freundlich constants which are related to sorption capacity and sorption intensity, respectively.

The correlation coefficients (R^2) of the linear form for Langmuir model were much closer to 1.0 than the values obtained with the Freundlich model. This was expectable based on the shape of sorption isotherms: the saturation plateau is consistent with the asymptotic trend associated to the Langmuir equation, while the Freundlich equation means an exponential trend. This suggests (to be verified by appropriate analytical procedures) that metal sorption occurs through monolayer sorption onto a surface, with a finite number of identical sites, which are homogeneously distributed over the sorbent surface. The experimental data were plotted as C_{eq}/q_e versus C_{eq} and shown in Figure AM3 (see additional material section). The parameters of the Langmuir model were used for simulating the sorption isotherms for the three sorbents at different temperatures: the solid lines fit well-experimental data (Fig. 9). Table 4 reports the values of Langmuir constants (i.e., q_{max} and b): both q_{max} and b increased with increasing temperature regardless of the sorbent. This means that Dy(III) binding on active sites of the sorbents becomes stronger at higher temperature and that the sorption process is endothermic. For the two parameters (maximum sorption capacity and affinity for Dy(III)), the sorbents can be classified according: cysteine > alanine > serine type. A tentative explanation for this difference in affinity has been presented above.

For further analysis on the sorption process, a dimensionless constant, R_L, which reflects the essential characteristic of Langmuir model, can be obtained from the constant b [55]:

$$R_L = \frac{1}{1 + bC_o} \tag{9}$$

where C_o is the initial concentration of the Dy(III) ion in the solution. The calculated values of the dimensionless factor R_L for the investigated sorbents toward the sorption of Dy(III) ions lie between 0.04 and 0.41 for alanine-functionalized sorbent, between 0.06 and 0.49 for serine-functionalized sorbent, and between 0.03 and 0.3 for cysteine-functionalized sorbent, regardless metal concentration and temperature. All R_L values were less than unity: this means that Dy(III) binding to the sorbents is a favorable sorption process.

The values of K_F, $1/n$ and R^2 in the Freundlich model are reported in Table 4 for alanine-, serine-, and cysteine-functionalized sorbents. The values of $1/n$ are less than 1.0 for all three sorbents, whatever the concentration and the temperature: this means that the sorption is a favorable process over the entire concentration range [55, 56].

The Dubinin–Radushkevich (D–R) isotherm model is usually employed for determining the physical or chemical nature of the sorption process. The D–R isotherm equation is given by [55, 57]

$$\ln q_e = \ln q_D - K\varepsilon^2 \tag{10}$$

where q_D is the theoretical saturation capacity, and ε is the Polanyi potential that is equal to [$\varepsilon = RT \ln(1 + 1/C_e)$]. K is related to the mean-free sorption energy per molecule of sorbate, E_{DR} (kJ/mol). E_{DR} provides information about chemical and physical sorption, and can be determined according to Eq. (11).

$$E_{DR} = (2K)^{-1/2} \tag{11}$$

Meanwhile, from the Dubinnin–Radushkevich (D–R) isotherm, the plot of ln q_e versus ε^2 gives a straight line with the slope K and the intercept ln q_D (Figure AM4, see additional material section). The parameters of the model are reported in Table 5. The mean sorption energy (E_{DR}) corresponds to the transfer of the free energy of 1 mol of solute from infinity (in solution) to the surface of the sorbent. The mean sorption energies (E_{DR}) of the Dy(III) ions for the three different sorbents are systematically below 8 kJ mol^{-1}; this shows that sorption proceeds through a physisorption mechanism [55, 57]. In addition, the positive value of E_{DR} means that the sorption process is endothermic. This is consistent with the improvement of sorption capacity with temperature (Fig. 9).

The Temkin isotherm supposes that the free energy of sorption is a function of the surface coverage [55, 58]. The model is described by

$$q_e = B_T \ln C_{eq} + B_T \ln A_T \tag{12}$$

where A_T is the equilibrium-binding constant (corresponding to the maximum binding energy: this reflects the initial sorption heat), B_T is the constant related to surface heterogeneity of the sorbent, T is the temperature (K), and R is the ideal gas constant (8.314 J mol^{-1} K^{-1}). The constants can be obtained from the slope and intercept of the straight line plot of q_e versus ln C_{eq}. The constants of the Temkin model are summarized in Table 5. The higher A_T value the higher sorption heat: the affinity of the sorbents for the solute increases with temperature [55]. The A_T values for the three functionalized materials obey the series: cysteine > alanine > serine, consistently with previous

Table 4 The Langmuir and Freundlich isotherms parameters of Dy(III) ions at different temperatures

Adsorbent	T K	$q_{max.}$ Exp.	Langmuir model			Freundlich model		
			$q_{max.Calc.}$	b (L mg^{-1})	R^2	$1/n$	K_F (mg g^{-1})	R^2
Alanine	300	14.8	16.0	0.052	0.997	0.237	4.25	0.940
	310	16.1	17.2	0.066	0.997	0.215	5.26	0.964
	320	17.2	18.2	0.080	0.998	0.209	5.87	0.953
Serine	300	8.93	10.0	0.038	0.996	0.277	2.08	0.960
	310	10.5	11.5	0.045	0.994	0.257	2.74	0.943
	320	11.5	12.4	0.056	0.998	0.252	3.15	0.934
Cysteine	300	17.6	18.6	0.086	0.999	0.221	5.79	0.949
	310	17.9	18.7	0.115	0.999	0.181	7.22	0.954
	320	18.3	18.9	0.151	0.999	0.167	7.99	0.950

Table 5 The D–R and Temkin isotherms parameters of Dy(III) ions at different temperatures

Adsorbent	D–R isotherm model					Temkin isotherm		
	T K	$q_{max.}$ (mg g^{-1})	$K_{ad} \times 10^4$ (mol^2 kJ^{-2})	E (KJ mol^{-1})	R^2	AT (L mg^{-1})	B_T (J mol^{-1})	R^2
Alanine	300	14.4	0.9	0.075	0.973	1.57	2.48	0.942
	310	15.6	0.6	0.091	0.904	2.69	2.51	0.956
	320	16.8	0.5	0.100	0.961	3.60	2.77	0.955
Serine	300	8.77	2.0	0.050	0.923	0.636	1.83	0.962
	310	10.2	1.0	0.071	0.807	0.927	2.01	0.940
	320	11.3	0.7	0.085	0.909	1.15	2.15	0.955
Cysteine	300	17.2	0.5	0.100	0.956	3.01	2.83	0.961
	310	17.6	0.3	0.129	0.972	9.77	2.42	0.960
	320	18.5	0.5	0.100	0.912	18.0	2.31	0.966

observations (such as comparison of maximum sorption capacities in the Langmuir model). Dy(III) ions were more likely to be bound on the cysteine than alanine type and serine-functionalized magnetic-chitosan sorbent, respectively.

The conclusions coming from uptake kinetics and sorption isotherms sound to be contradictory. Indeed, the PSORE model is generally associated to a chemisorption process (controlled by the mechanism of electron sharing, or exchange between sorbent surface and sorbate), while the mean sorption energies (E_{DR}) (being less than 8 kJ mol^{-1}) come along with physisorption process. This suggests that a dual mechanism is involved in Dy(III) sorption when using the functionalized materials [4]: a physical sorption (electrostatic forces) takes place at low-metal concentration followed by a chemical sorption (ionic forces: coordination) at higher metal concentration.

Effect of temperature and thermodynamic studies

The effect of temperature on the sorption of Dy(III) ions on the three sorbents was investigated at 300, 310, and 320 K. The values of q_m as a function of temperature are plotted in Figure AM5 (see additional material section). The amounts of sorbed metal ions increased gradually with rising the temperature, as expected by the calculated values of b and E_{DR}: the sorption process is endothermic. This was mainly attributed to the increase in the Lewis acid–base interaction between metal ions and ligands on sorbent surface as the temperature raises [14]. This behavior was also associated to (a) a higher probability of collision between metal ions and the sorbent surface and (b) a stronger driving force, which lessens the mass-transfer resistance [59].

The experimental data obtained at different temperatures were used for calculating the thermodynamics parameters: standard Gibbs free energy change (ΔG°), enthalpy change (ΔH°), and entropy change (ΔS°) were derived from van't Hoff equation.

$$\ln b = \frac{-\Delta H^\circ}{\mathrm{RT}} + \frac{\Delta S^\circ}{R} \tag{13}$$

$$\Delta G^\circ = \Delta H^\circ - T\Delta S^\circ \tag{14}$$

where b is the equilibrium constant (obtained from Langmuir isotherms at different temperatures) and T is absolute

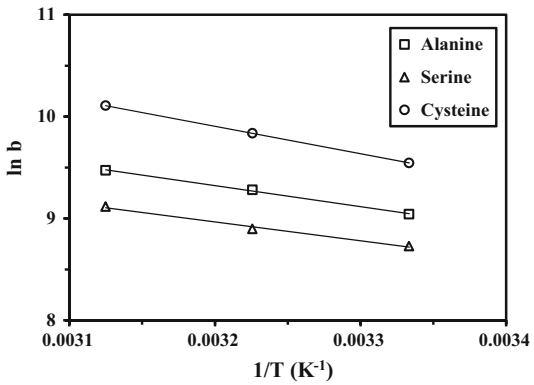

Fig. 10 Van't Hoff plots of ln b against 1/T, (K^{-1}) for Dy(III) sorption using alanine-, serine-, and cysteine-functionalized magnetic-chitosan nano-based particles

temperature (Kelvin). The values of enthalpy change ($\Delta H°$) and entropy change ($\Delta S°$) were obtained by plotting ln b against 1/T (Fig. 10). The values of $\Delta H°$, $\Delta S°$, and $\Delta G°$ are reported in Table 6. The sorption of Dy(III) ions on the three sorbents is endothermic: the positive value of $\Delta H°$, the negative value of free energy, and the decrease in the value of $\Delta G°$ with increase in temperature show that the reaction is enhanced at high temperature. The positive value of $\Delta S°$ may be related to the liberation of water of hydration during the sorption process causing the increase in the randomness of the system. Metal ions are hydrated in aqueous media, their sorption at the surface of the sorbent causes the release of water molecules, and the entropy of the system increases. Also the data showed the $|\Delta H°| < |T\Delta S°|$ in the studied temperature range. This indicated that the sorption process was dominated by entropic rather than enthalpic changes [60].

Comparison of sorption properties with conventional sorbents

Depending on the type of acid used for grafting on chitosan magnetic backbone, the maximum sorption capacity varies between 9 and 18 mg Dy g^{-1}. These values are relatively low compared to conventional materials (some data are reported in Table 7). Since the experimental conditions are not identical (metal range, sorbent dosage, contact, time, pH, and solution composition), a direct comparison is not easy; however, these low values can be explained by the huge amount of magnetic core (which counts for about

Table 6 Thermodynamic parameters of Dy(III) ions by the three different sorbents

Adsorbent	ΔH (kJ mol^{-1})	ΔS (J mol^{-1} K^{-1})	T K	ΔG (kJ mol^{-1})	$T\Delta S$ (kJ mol^{-1})	R^2
Alanine	17.2	133	300	−22.6	39.9	0.998
			310	−23.9	41.2	
			320	−25.2	42.6	
Serine	15.5	124	300	−21.8	37.2	0.992
			310	−23.0	38.4	
			320	−24.2	39.7	
Cysteine	22.5	154	300	−23.8	46.2	0.999
			310	−25.4	47.7	
			320	−26.9	49.3	

Table 7 Comparison of Dy(III) sorption properties for different sorbents

Sorbent	Range of contact time (h)	pH range	q_m (mg Dy g^{-1})	References
Activated-charcoal	0.7–1	4	294	[61]
Ion-imprinted polymer	0.17[a]	6–9	40	[62]
D113 resin (carboxylate groups)	>40	6	293	[63]
Oxidized multi-walled carbon nanotubes	1	–	78	[64]
Mesoporous silica microspheres and xerogels impregnated with phosphonic groups	0.5/>40[b]	3–5	48	[65, 66]
Molybdo-vanadophosphoric acid supported on Zr modified mesoporous silica SBA-15	1	5	37–53	[67]
Dried or carbonized parachlorella/clay mineral	2	7	0.2–1.4	[68]
Amino-acid functionalized chitosan magnetic nano-based particles	4–5	5–6	9–18	This work

[a] Incomplete information

[b] Depending on the conditioning of the material (microspheres vs. xerogels)

Table 8 Adsorption–desorption cycles of the three different sorbents

Cycle	Alanine		Serine		Cysteine	
	q_e (mg Dy g^{-1})	Ads. (%)	q_e (mg Dy g^{-1})	Ads. (%)	q_e (mg Dy g^{-1})	Ads. (%)
I	12.8	100	7.34	100	15.8	100
II	12.2	95.5	7.09	96.6	14.8	94.0
III	12.2	95.2	7.06	96.2	14.7	93.5
IV	12.1	94.6	6.99	95.2	14.6	92.8

50 % of the total mass of sorbent). A way to improve the sorption performance would consist in optimizing the amount of magnetite in the hybrid material. This optimization should take into account both optimized sorption capacities and also good magnetic properties: this means that a substantial amount of magnetite is required. The weak sorption properties (in terms of capacities) are partially compensated by the relatively fast uptake kinetics that is enhanced by the sub-micron size of sorbent particles.

Regeneration studies

Acidic solutions are frequently used for desorption of metal ions immobilized on sorbents and resins. In the present case, the magnetic core constituted of Fe_3O_4 is very sensitive to drastic acidic conditions. It is thus necessary evaluating alternative eluents, especially strong complexing agents such as ethylenediamine tetraacetic acid (EDTA) and thiourea. These strong metal-chelating agents will displace the sorption equilibrium toward metal release. Table 8 reports the evolution of sorption capacity and sorption efficiency for four sorption/desorption cycles. A slight decrease of sorption performance is observed but even at the fourth step the decrease in sorption efficiency is less than 7 %. In terms of feasibility and efficiency of desorption, the materials can be classified according: alanine- $\approx$ serine- $>$ cysteine-functionalized magnetic-chitosan sorbents. Sulfur-reactive groups are generally very strong-binding agents and their regeneration is frequently difficult; in addition, these materials may be subject to chemical degradation. These reasons could explain the slight difference in the desorption properties. It is noteworthy that even with this material, the sorption efficiency at the fourth step remains close to 93 % of the initial value. So, the desorption performance remains appreciable.

Conclusion

In this study, three different chelating sorbents were synthesized (alanine/serine/cysteine moieties were grafted on chitosan previously coated on magnetite nanoparticles). These materials have super-paramagnetic properties and they have affinity for Dy(III) binding from aqueous solutions. The Langmuir model fits well-experimental sorption data for Dy(III). The maximum sorption capacities were found to be 14.8, 8.9, and 17.6 mg Dy g^{-1} for alanine, serine, and cysteine type, respectively, at pH 5. The values of Gibbs energy ($\Delta G°$) and reaction enthalpy ($\Delta H°$) indicate the spontaneous and endothermic nature, while the positive value of entropy ($\Delta S°$) indicates increased randomness due to sorption. Finally, the sorbent can be regenerated with high efficiency by acidified 0.5 M thiourea as an eluent; and after three cycles, the sorption capacities are not significantly reduced.

Despite the interest and performance of these materials, the number of successive steps to be implemented for the manufacturing of the sorbent makes the materials relatively expensive and their application limited to very specific applications such as treatment of metal-containing solutions in hazardous environments (nuclear industry), for the recovery of noble and strategic metals (platinum-group metals, PGMs), or for the design of advanced materials (such as synthesis of nano-sized magnetic supports for heterogeneous catalysis, immobilizing PGMs).

Acknowledgements This research was supported by the French Government through a fellowship granted from the French Embassy in Egypt (Institut Français d'Égypte). A special dedication is given to memory of Dr. Ahmed Donia.

References

1. Fu F, Wang Q (2011) Removal of heavy metal ions from wastewaters: a review. J Environ Manage 92(3):407–418. doi:10.1016/j.jenvman.2010.11.011
2. Bailey SE, Olin TJ, Bricka RM, Adrian DD (1999) A review of potentially low-cost sorbents for heavy metals. Water Res 33(11):2469–2479. doi:10.1016/s0043-1354(98)00475-8
3. Zhou L, Liu Z, Liu J, Huang Q (2010) Adsorption of Hg(II) from aqueous solution by ethylenediamine-modified magnetic cross-linking chitosan microspheres. Desalination 258(1–3):41–47. doi:10.1016/j.desal.2010.03.051
4. Hu X-J, Wang J-S, Liu Y-G, Li X, Zeng G-M, Bao Z-L, Zeng X-X, Chen A-W, Long F (2011) Adsorption of chromium (VI) by ethylenediamine-modified cross-linked magnetic chitosan resin:

Isotherms, kinetics and thermodynamics. J Hazard Mater 185(1):306–314. doi:10.1016/j.jhazmat.2010.09.034
5. Navarro R, Saucedo I, Gonzalez C, Guibal E (2012) Amberlite XAD-7 impregnated with Cyphos IL-101 (tetraalkylphosphonium ionic liquid) for Pd(II) recovery from HCl solutions. Chem Eng J 185–186:226–235. doi:10.1016/j.cej.2012.01.090
6. Chassary P, Vincent T, Sanchez Marcano J, Macaskie LE, Guibal E (2005) Palladium and platinum recovery from bicomponent mixtures using chitosan derivatives. Hydrometallurgy 76(1–2):131–147. doi:10.1016/j.hydromet.2004.10.004
7. Gurung M, Adhikari BB, Kawakita H, Ohto K, Inoue K, Alam S (2013) Recovery of gold and silver from spent mobile phones by means of acidothiourea leaching followed by adsorption using biosorbent prepared from persimmon tannin. Hydrometallurgy 133:84–93. doi:10.1016/j.hydromet.2012.12.003
8. Mack C, Wilhelmi B, Duncan JR, Burgess JE (2007) Biosorption of precious metals. Biotechnol Adv 25(3):264–271. doi:10.1016/j.biotechadv.2007.01.003
9. Donia AM, Atia AA, Elwakeel KZ (2007) Recovery of gold(III) and silver(I) on a chemically modified chitosan with magnetic properties. Hydrometallurgy 87(3–4):197–206. doi:10.1016/j.hydromet.2007.03.007
10. Oliveira RC, Jouannin C, Guibal E, Garcia O Jr (2011) Samarium(III) and praseodymium(III) biosorption on *Sargassum sp.*: batch study. Proc Biochem 46(3):736–744. doi:10.1016/j.procbio.2010.11.021
11. Oliveira RC, Hammer P, Guibal E, Taulemesse J-M, Garcia O Jr (2014) Characterization of metal–biomass interactions in the lanthanum(III) biosorption on *Sargassum sp.* using SEM/EDX, FTIR, and XPS: preliminary studies. Chem Eng J 239:381–391. doi:10.1016/j.cej.2013.11.042
12. Oliveira RC, Guibal E, Garcia O Jr (2012) Biosorption and desorption of lanthanum(III) and neodymium(III) in fixed-bed columns with *Sargassum sp.*: perspectives for separation of rare earth metals. Biotechnol Progr 28(3):715–722. doi:10.1002/btpr.1525
13. Wang J-S, Peng R-T, Yang J-H, Liu Y-C, Hu X-J (2011) Preparation of ethylenediamine-modified magnetic chitosan complex for adsorption of uranyl ions. Carbohydr Polym 84(3):1169–1175. doi:10.1016/j.carbpol.2011.01.007
14. Wang H, Ma L, Cao K, Geng J, Liu J, Song Q, Yang X, Li S (2012) Selective solid-phase extraction of uranium by salicylideneimine-functionalized hydrothermal carbon. J Hazard Mater 229:321–330. doi:10.1016/j.jhazmat.2012.06.004
15. Roig MG, Manzano T, Diaz M (1997) Biochemical process for the removal of uranium from acid mine drainages. Water Res 31(8):2073–2083. doi:10.1016/s0043-1354(97)00036-5
16. De Corte S, Hennebel T, De Gusseme B, Verstraete W, Boon N (2012) Bio-palladium: from metal recovery to catalytic applications. Microb Biotechnol 5(1):5–17. doi:10.1111/j.1751-7915.2011.00265.x
17. Lokshin EP, Ivanenko VI, Tareeva OA, Korneikov RI (2013) Sorption of rare earth elements of waste solution of leaching uranium. Russ J Appl Chem 86(3):450–452. doi:10.1134/s1070427213030269
18. Roosen J, Binnemans K (2014) Adsorption and chromatographic separation of rare earths with EDTA- and DTPA-functionalized chitosan biopolymers. J Mater Chem A 2(5):1530–1540. doi:10.1039/c3ta14622g
19. Wang GH, Liu JS, Wang XG, Xie ZY, Deng NS (2009) Adsorption of uranium (VI) from aqueous solution onto cross-linked chitosan. J Hazard Mater 168(2–3):1053–1058. doi:10.1016/j.jhazmat.2009.02.157
20. Starvin AM, Rao TP (2004) Solid phase extractive preconcentration of uranium(VI) onto diarylazobisphenol modified activated carbon. Talanta 63(2):225–232. doi:10.1016/j.talanta.2003.11.001
21. Donia AM, Atia AA, Abouzayed FI (2012) Preparation and characterization of nano-magnetic cellulose with fast kinetic properties towards the adsorption of some metal ions. Chem Eng J 191:22–30. doi:10.1016/j.cej.2011.08.034
22. Rao TP, Metilda P, Gladis JM (2006) Preconcentration techniques for uranium(VI) and thorium(IV) prior to analytical determination—an overview. Talanta 68(4):1047–1064. doi:10.1016/j.talanta.2005.07.021
23. Guibal E (2004) Interactions of metal ions with chitosan-based sorbents: a review. Sep Purif Technol 38(1):43–74. doi:10.1016/j.seppur.2003.10.004
24. Mata YN, Blazquez ML, Ballester A, Gonzalez F, Munoz JA (2009) Sugar-beet pulp pectin gels as biosorbent for heavy metals: preparation and determination of biosorption and desorption characteristics. Chem Eng J 150(2–3):289–301. doi:10.1016/j.cej.2009.01.001
25. Martinez RE, Pourret O, Takahashi Y (2014) Modeling of rare earth element sorption to the Gram positive *Bacillus subtilis* bacteria surface. J Colloid Interface Sci 413:106–111. doi:10.1016/j.jcis.2013.09.037
26. Zhou L, Xu J, Liang X, Liu Z (2010) Adsorption of platinum(IV) and palladium(II) from aqueous solution by magnetic cross-linking chitosan nanoparticles modified with ethylenediamine. J Hazard Mater 182(1–3):518–524. doi:10.1016/j.jhazmat.2010.06.062
27. Gao YH, Oshita K, Lee KH, Oshima M, Motomizu S (2002) Development of column-pretreatment chelating resins for matrix elimination/multi-element determination by inductively coupled plasma-mass spectrometry. Analyst 127(12):1713–1719. doi:10.1039/b208341h
28. Oshita K, Sabarudin A, Takayanagi T, Oshima M, Motomizu S (2009) Adsorption behavior of uranium(VI) and other ionic species on cross-linked chitosan resins modified with chelating moieties. Talanta 79(4):1031–1035. doi:10.1016/j.talanta.2009.03.035
29. Jayakumar R, Prabaharan M, Reis RL, Mano JF (2005) Graft copolymerized chitosan—present status and applications. Carbohydr Polym 62(2):142–158. doi:10.1016/j.carbpol.2005.07.017
30. Xue X, Wang J, Mei L, Wang Z, Qi K, Yang B (2013) Recognition and enrichment specificity of Fe_3O_4 magnetic nanoparticles surface modified by chitosan and *Staphylococcus aureus* enterotoxins A antiserum. Colloids Surf B 103:107–113. doi:10.1016/j.colsurfb.2012.10.013
31. Moldoveanu GA, Papangelakis VG (2012) Recovery of rare earth elements adsorbed on clay minerals: I. Desorption mechanism. Hydrometallurgy 117:71–78. doi:10.1016/j.hydromet.2012.02.007
32. Cotton S (2006) Lanthanide and actinide chemistry. Wiley, Chichester
33. Diniz V, Volesky B (2005) Biosorption of La, Eu and Yb using *Sargassum* biomass. Water Res 39(1):239–247. doi:10.1016/j.waters.2004.09.009
34. Donia AM, Atia AA, Daher AM, Desouky OA, Elshehy EA (2011) Synthesis of amine/thiol magnetic resin and study of its interaction with Zr(IV) and Hf(IV) ions in their aqueous solutions. J Dispers Sci Technol 32(5):634–641. doi:10.1080/01932691003799860
35. Filha V, Wanderley AF, de Sousa KS, Espinola JGP, da Fonseca MG, Arakaki T, Arakaki LNH (2006) Thermodynamic properties of divalent cations complexed by ethylenesulfide immobilized on silica gel. Colloids Surf A 279(1–3):64–68. doi:10.1016/j.colsurfa.2005.12.041
36. Massart R (1981) Preparation of aqueous magnetic liquids in alkaline and acidic media. IEEE Trans Magn 17(2):1247–1249

37. Namdeo M, Bajpai SK (2008) Chitosan-magnetite nanocomposites (CMNs) as magnetic carrier particles for removal of Fe(III) from aqueous solutions. Colloids Surf A 320(1–3):161–168. doi:10.1016/j.colsurfa.2008.01.053
38. Wan Ngah WS, Endud CS, Mayanar R (2002) Removal of copper(II) ions from aqueous solution onto chitosan and cross-linked chitosan beads. React Funct Polym 50(2):181–190
39. Oshita K, Takayanagi T, Oshima M, Motomizu S (2007) Adsorption behavior of cationic and anionic species on chitosan resins possessing amino acid moieties. Anal Sci 23(12):1431–1434. doi:10.2116/analsci.23.1431
40. Gonçalves VL, Laranjeira MCM, Fávere VT, Pedrosa RC (2005) Effect of crosslinking agents on chitosan microspheres in controlled release of diclofenac sodium. Polim: Cienc Tecnol 15(1):6–12. doi:10.1590/s0104-14282005000100005
41. Dong C, Chen W, Liu C, Liu Y, Liu H (2014) Synthesis of magnetic chitosan nanoparticle and its adsorption property for humic acid from aqueous solution. Colloids Surf A 446:179–189. doi:10.1016/j.colsurfa.2014.01.069
42. Oshita K, Oshima M, Gao YH, Lee KH, Motomizu S (2003) Synthesis of novel chitosan resin derivatized with serine moiety for the column collection/concentration of uranium and the determination of uranium by ICP-MS. Anal Chim Acta 480(2):239–249. doi:10.1016/s0003-2670(03)00020-5
43. Coates J (2000) Interpretation of infrared spectra, a practical approach. In: Meyers RA (ed) Encyclopedia of analytical chemistry. Wiley, Chichester, pp 10815–10837
44. Zhang X, Jiao C, Wang J, Liu Q, Li R, Yang P, Zhang M (2012) Removal of uranium(VI) from aqueous solutions by magnetic Schiff base: kinetic and thermodynamic investigation. Chem Eng J 198:412–419. doi:10.1016/j.cej.2012.05.090
45. Hosoba M, Oshita K, Katarina RK, Takayanagi T, Oshima M, Motomizu S (2009) Synthesis of novel chitosan resin possessing histidine moiety and its application to the determination of trace silver by ICP-AES coupled with triplet automated-pretreatment system. Anal Chim Acta 639(1–2):51–56. doi:10.1016/j.aca.2009.02.050
46. Guinier A, Lorrain P, Sainte-Marie Lorrain D (1963) X-ray diffraction: in crystals, imperfect crystals and amorphous bodies. W.H. Freeman & Co, San Francisco
47. Bhatt AS, Krishna Bhat D, Santosh MS (2010) Electrical and magnetic properties of chitosan-magnetite nanocomposites. Phys B 405(8):2078–2082. doi:10.1016/j.physb.2010.01.106
48. Yan H, Li H, Yang H, Li A, Cheng R (2013) Removal of various cationic dyes from aqueous solutions using a kind of fully biodegradable magnetic composite microsphere. Chem Eng J 223:402–411. doi:10.1016/j.cej.2013.02.113
49. Pearson RG (1966) Acids and bases. Science 151(3707):172–177. doi:10.1126/science.151.3707.172
50. Awual MR, Kobayashi T, Miyazaki Y, Motokawa R, Shiwaku H, Suzuki S, Okamoto Y, Yaita T (2013) Selective lanthanide sorption and mechanism using novel hybrid Lewis base (N-methyl-N-phenyl-1,10-phenanthroline-2-carboxamide) ligand modified adsorbent. J Hazard Mater 252–253:313–320. doi:10.1016/j.jhazmat.2013.03.020
51. Yang YJ, Alexandratos SD (2009) Affinity of polymer-supported reagents for lanthanides as a function of donor atom polarizability. Ind Eng Chem Res 48(13):6173–6187. doi:10.1021/ie900074t
52. Qiu H, Lv L, Pan B, Zhang Q, Zhang W, Zhang Q (2009) Review: critical review in adsorption kinetic models. J Zhejiang Univ Sci A 10:716–724
53. Plazinski W, Dziuba J, Rudzinski W (2013) Modeling of sorption kinetics: the pseudo-second order equation and the sorbate intraparticle diffusivity. Adsorption 19(5):1055–1064. doi:10.1007/s10450-013-9529-0
54. Langmuir I (1918) The adsorption of gases on plane surfaces of glass, mica and platinum. J Am Chem Soc 40:1361–1402
55. Foo KY, Hameed BH (2010) Insights into the modeling of adsorption isotherm systems. Chem Eng J 156(1):2–10. doi:10.1016/j.cej.2009.09.013
56. Freundlich HMF (1906) Uber die adsorption in lasungen. Z Phys Chem 57:385–470
57. Dubinin MM, Zaverina ED, Radushkevich LV (1947) Sorption and structure of active carbons. I. Adsorption of organic vapors. Zh Fiz Khim 21:1351–1362
58. Temkin VP (1940) Kinetics of ammonia synthesis on promoted iron catalysts. Acta Physiochim 12:217–222
59. Ozsoy HD, Kumbur H (2006) Adsorption of Cu(II) ions on cotton boll. J Hazard Mater 136(3):911–916. doi:10.1016/j.jhazmat.2006.01.035
60. Rahmati A, Ghaemi A, Samadfam M (2012) Kinetic and thermodynamic studies of uranium(VI) adsorption using Amberlite IRA-910 resin. Ann Nucl Energy 39(1):42–48. doi:10.1016/j.anucene.2011.09.006
61. Qadeer R, Hanif J (1995) Adsorption of dysprosium ions on activated-charcoal from aqueous solutions. Carbon 33(2):215–220. doi:10.1016/0008-6223(94)00135-m
62. Biju VM, Gladis JM, Rao TP (2003) Ion imprinted polymer particles: synthesis, characterization and dysprosium ion uptake properties suitable for analytical applications. Anal Chim Acta 478(1):43–51. doi:10.1016/s0003-2670(02)01416-2
63. Wang H, Gao P (2007) Adsorption of D113 resin for dysprosium(III). J Wuhan Univ Technol—Mater SciEd 22(4):653–656. doi:10.1007/s11595-006-4653-2
64. Koochaki-Mohammadpour SMA, Torab-Mostaedi M, Talebizadeh-Rafsanjani A, Naderi-Behdani F (2014) Adsorption isotherm, kinetic, thermodynamic, and desorption studies of lanthanum and dysprosium on oxidized multiwalled carbon nanotubes. J Disper Sci Technol 35(2):244–254. doi:10.1080/01932691.2013.785361
65. Melnyk IV, Goncharyk VP, Kozhara LI, Yurchenko GR, Matkovsky AK, Zub YL, Alonso B (2012) Sorption properties of porous spray-dried microspheres functionalized by phosphonic acid groups. Microporous Mesoporous Mater 153:171–177. doi:10.1016/j.micromeso.2011.12.027
66. Melnyk IV, Goncharyk VP, Stolyarchuk NV, Kozhara LI, Lunochkina AS, Alonso B, Zub YL (2012) Dy(III) sorption from water solutions by mesoporous silicas functionalized with phosphonic acid groups. J Porous Mater 19(5):579–585. doi:10.1007/s10934-011-9508-3
67. Aghayan H, Mahjoub AR, Khanchi AR (2013) Samarium and dysprosium removal using 11-molybdo-vanadophosphoric acid supported on Zr modified mesoporous silica SBA-15. Chem Eng J 225:509–519. doi:10.1016/j.cej.2013.03.092
68. Ponou J, Wang LP, Dodbiba G, Okaya K, Fujita T, Mitsuhashi K, Atarashi T, Satoh G, Noda M (2014) Recovery of rare earth elements from aqueous solution obtained from Vietnamese clay minerals using dried and carbonized parachlorella. J Environ Chem Eng 2(2):1070–1081. doi:10.1016/j.jece.2014.04.002